Assessment of a Support System for Squeezing Rock Conditions by means of a Hybrid Method

By Jürgen Macht, Christian Hellmich, Roman Lackner, Wulf Schubert and Herbert A. Mang

In case of tunnelling in squeezing rock, e.g., when passing fault zones under high overburden, relatively large displacements of the rock mass are recorded. Then, the rigidity of conventional tunnel linings may be the reason for considerable damage of the tunnel lining.

Hence, for such ground conditions, the development of alternative tunnel support systems was highly desirable. As early as 1975, Rabcewicz (14) reported on a successful remedy used at the Tauerntunnel: Longitudinal gaps were left in the linings in order to allow for remarkable circumferential displacements without damage of the shotcrete tunnel lining. In this case, the circumferential axial forces in the tunnel lining are induced by shear forces at the interface of the shotcrete segments and the adjacent rock, which are connected by a dense grid of rock bolts.

Later, attempts were made to determine characteristic values for the circumferential axial forces in the shotcrete segments. In (13), a Mohr-Coulomb friction law is used for the description of the shotcrete-rock interface. Based on estimates for the cohesion c and the angle of internal friction φ, very low values were calculated for the shear forces at the interface and, hence, for the circumferential axial forces in such a tunnel lining. In view of the strong anisotropy and inhomogeneity of the rock and the inaccessibility of the respective interface in situ, it is next to impossible to determine the material parameters c and φ experimentally.

However, assuming a very low degree of utilization, which, roughly speaking, is equal to the circumferential stress in the tunnel lining divided by the current strength, the tunnel support

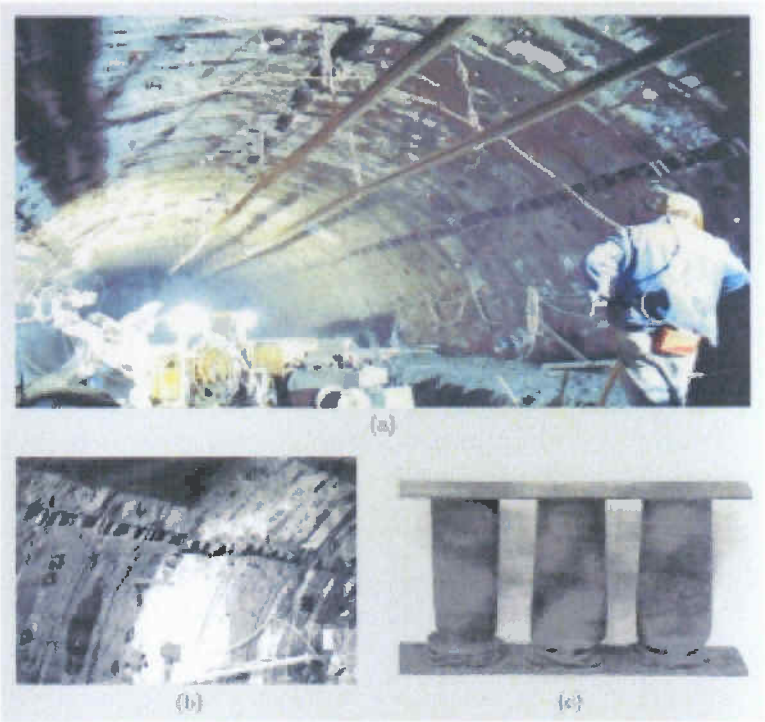

Fig. 1 Semmering pilot tunnel: (a, b) shotcrete tunnel lining with Lining Stress Controllers (LSC) installed in longitudinal gaps and (c) prototype of LSC after buckling (15).

Bild 1 *Semmering-Pilotstollen: (a, b) Spritzbetonschale mit in Lngsschlitzen angeordneten Stauchelementen (LSC) und (c) Prototyp eines Stauchelements (15).*

Bewertung eines Tunnelausbaus für druckhaftes Gebirge mittels einer hybriden Methode

Beim Vortrieb von Tunneln in druckhaftem Gebirge werden relativ große Verschiebungen des umliegenden Gebirges aufgezeichnet. Unter diesen Bedingungen kann die verhältnismäßig große Steifheit eines konventionellen Ausbaus zu beachtlicher Schädigung der Tunnelschale führen. Als Abhilfe wurden schon 1972 Längsschlitze in Tunnelschalen aus Spritzbeton angeordnet. Die Schlitze lassen relativ große Umfangsverschiebungen ohne Schädigung der Tunnelschale zu. Die Ausrüstung der Längsschlitze mit Dämpfelementen aus Stahl ermöglicht eine Kraftübertragung über die Schlitze hinweg. Zum Verständnis der Wirkungsweise und zur Bewertung eines solchen Ausbausystems wird eine hybride Methode zur Quantifizierung von Spannungszuständen in Spritzbetontunnelschalen angewendet.

In case of tunnelling in squeezing rock, relatively large displacements of the rock mass are recorded. In this case, the rigidity of conventional tunnel linings may cause considerable damage of the tunnel lining. As a remedy, already in 1972, longitudinal gaps were left in the linings in order to allow for relatively large circumferential displacements without damage of the shotcrete tunnel lining. In this case, the circumferential axial forces in the tunnel lining are transferred through shear forces at the interface of the shotcrete segments and the adjacent rock, which are connected by a dense grid of rock bolts. By installing steel damping elements in the longitudinal gaps, circumferential axial forces can be transferred over the gaps. In order to understand such a tunnel support system and to assess its functionality, a hybrid method for the quantification of stress states in shotcrete tunnel linings is applied.

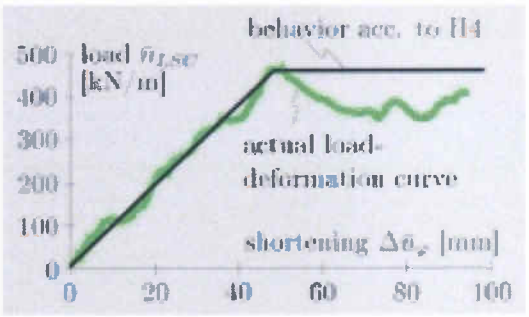

Fig. 2 Semmering pilot tunnel: experimentally obtained relation between the shortening of the LSC, type 2AI, $\Delta\bar{u}_{\varphi}$, and the applied load, $\bar{n}_{LSC}$ (12).

Bild 2 *Semmering-Pilotstollen: experimentell ermitteltes Last-Verformungs-(n-u)-Diagramm fr ein Stauchelement, Typ 2AI.*

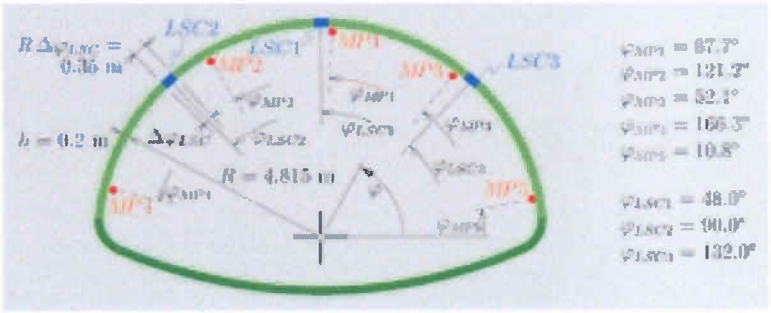

Fig. 3 Location of measurement points (MP) and Lining Stress Controllers (LSC) in the Semmering pilot tunnel at km 4.274.

Bild 3 *Lage der Mepunkte (MP) und der Stauchelemente (LSC) im Semmering-Pilotstollen (km 4.274).*

system was further improved by installing damping elements within the longitudinal gaps (12, 15, 17). In this way, circumferential axial forces can be transferred over the gaps. Thus, the degree of utilization is increased. The damping elements are called Lining Stress Controllers (LSC). In the given case, steel cylinders are used as LSCs (Figure 1). Their load-deformation behaviour is nearly bilinear (Figure 2). The LCSs are functioning as follows: In principle, loading of a tunnel lining may be regarded as a displacement-driven process. Before the strength of shotcrete is reached in this process, the LSCs are buckling. This results in large circumferential shortening in the longitudinal gaps of the lining. According to (12), from this point on, the circumferential axial forces in the tunnel lining are controlled by the LSC behaviour.

Up to now the design of the LSCs is based on the hypothesis that the shear force between lining and rock in squeezing ground is negligible. In order to validate this hypothesis, an attempt was made to quantify the stress state of a segmented shotcrete lining with LSCs installed in the gaps with the help of a hybrid method. A case example from the pilot tunnel of the Semmering base tunnel in Austria is used, where this type of support was installed and displacement monitoring data are available.

Hybrid method for quantification of stress states in shotcrete tunnel linings

This hybrid method constitutes a combination of 3D displacement measurements with thermo-chemomechanical material modelling of shotcrete in the framework of the non-linear Finite Element Method (3, 5). This method comprises the following steps:

- Formulation of hypotheses concerning the structural behaviour of the tunnel lining ("structural hypotheses") .
- Investigation of the tunnel lining on the basis of a ring with a width of 1 m, which is fictitiously cut out of the lining structure. This part of the tunnel lining is modelled by means of 3D or 2D plane strain Finite Elements on the basis of the structural hypotheses.
- Approximation of the fields of displacement components at surfaces at which forces are introduced into the lining structure. These approximations are made on the basis of (a) in-situ displacement measurements at discrete points of the lining and (b) the structural hypotheses. The approximated displacement fields serve as boundary conditions for the FE model of the investigated part of the tunnel lining.

Based on statements in (13) on the low shear forces at the shotcrete-rock interface, the structural hypothesis of a frictionless relative movement between shotcrete and rock at this interface was formulated in (10). It was tested for the cross section km 4.274 of the Semmering pilot tunnel (Figure 3). In this analysis only the radial displacement states were prescribed. The numerically obtained circumferential displacement states of the interior surface of the tunnel lining did not agree with the respective displacements measured on site (10). Consequently, in contrast

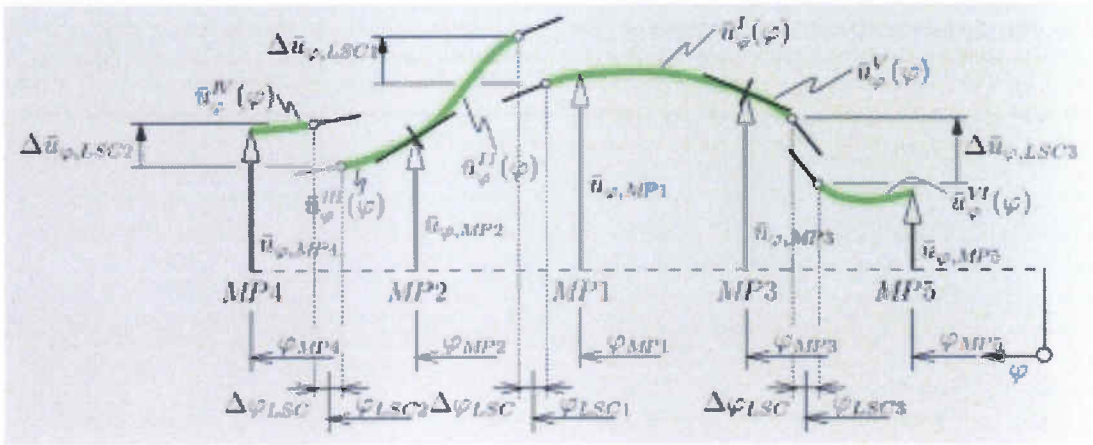

Fig. 4 Illustration of the quadratic interpolation of the circumferential displacements $\bar{u}_{\varphi}$ on the basis of displacements at measurement points MP1 to MP5, displacement jumps and prescribed values of $\bar{u}'_{\varphi} = \partial\bar{u}_{\varphi}/\partial\varphi$ at LSC1 to LSC3 (8). $\Delta\varphi$ refers to the gap in the shotcrete lining, where the LSCs are placed. For the Semmering pilot tunnel, $\Delta\varphi = 2.04°$, $\bar{u}'_{\varphi} = \partial\bar{u}_{\varphi}/\partial\varphi$.

Bild 4 *Darstellung der quadratischen Interpolation der Umfangsverschiebungen $\bar{u}_{\varphi}$ unter Zugrundelegung der in MP1 bis MP5 gemessenen Verschiebungen sowie der bei LSC1 bis LSC3 gemessenen Verschiebungssprnge und der dort vorgeschriebenen Werte $\bar{u}'_{\varphi} = \partial\bar{u}_{\varphi}/\partial\varphi$ (8). $\Delta\varphi$ bezieht sich auf die Lngsschlitze in der Tunnelschale, in denen die LSC plaziert sind ($\Delta\varphi = 2.04$ fr den Semmering-Pilotstollen).*

to the statements in (13), the shear forces at the interface are most probably not negligible.

Thus, the hypothesis of negligible shear forces was replaced by more realistic hypotheses. This has led to a structural model characterized by the following hypotheses (11):

- H1: During the deformation, the thickness of the lining is assumed to be approximately constant. Because of the small thickness and the mode of loading of the lining, this assumption is justified.
- H2: As for the parts of the lining made of shotcrete, smooth displacement fields are assumed. With regards to the gaps, after buckling of the LSCs (see localized deformation in Figure 1c), large displacement gradients occur in a very small region as compared to the dimensions of the whole structure. This situation can be approximated by discontinuous displacement fields. These fields exhibit a jump in the circumferential direction.
- H3: There is no stress transfer between the footing of the top heading support and the adjacent rock.
- H4: The load-deformation characteristics of the LSCs are assumed to be linear-elastic – ideally-plastic. In other words, they have a well-defined ultimate load for a large range of (non-elastic) deformations (12). The experimental load-displacement curve for the LSCs used at the Semmering pilot tunnel is depicted in Figure 2.
- H5: The bending moment which can be taken by the LSCs is negligible in comparison to the one which can be taken by the shotcrete lining. Hence, zero values for the bending moment are assumed at the shotcrete-LSC interface.

The algorithmic realization of H1-H5 requires the development of numerous advanced numerical tools, which are described in detail in (8). To give a rough idea on this algorithmic investigation, Figures 4 and 5 illustrate the employed approximation of the radial and circumferential displacement fields by means of quadratic interpolation functions. Quantities with the indices MPi, i=1, 2, 3, 4, 5, or LCSj, j=1, 2, 3 indicate measured values. Figure 6 shows the in-plane measurement traces of the five measurement points.

The second foundation of the hybrid method is advanced material modelling of shotcrete. Such a material model was developed and continuously improved at the Institute for Strength of Materials over the last half decade (1, 2, 4, 6, 7, 16):

Shotcrete is modelled in the framework of chemically reactive porous media. Dissipative phenomena at the microlevel of the material are accounted for by means of (internal) state variables and energetically conjugated thermodynamic forces, related to the state variables via state equations. The rates of the internal state variables are related to the corresponding thermodynamic forces by means of appropriate evolution equations.

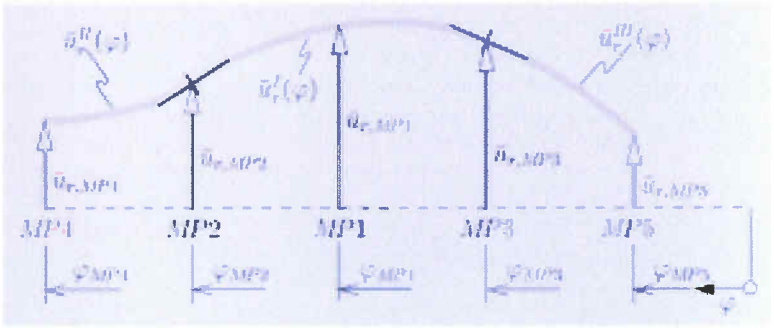

Fig. 5 Illustration of the quadratic interpolation of the radial displacements $\bar{u}_r$ on the basis of displacements at measurement points MP1 to MP5 (8).

Bild 5 *Darstellung der quadratischen Interpolation der Radialverschiebungen $\bar{u}_r$ zwischen den in MP1 bis MP5 gemessenen Verschiebungen (8).*

The following dissipative phenomena govern the material behaviour:

- The chemical reaction between water and cement, i.e., hydration, results in chemical shrinkage strains, ageing elasticity, strength growth (chemomechanical couplings), and in latent heat production (thermochemical coupling). The state of the reaction is described by the mass per unit volume of the reaction products called hydrates and denoted as m.
- Microcracking of the hydrates leads to plastic strains ε^p. The state of microstructural changes resulting from microcracking (i.e., hardening/softening) is described by hardening variables χ, as in classical plasticity theory. In the present case, a multisurface model consisting of a Drucker-Prager loading surface and three Rankine loading surfaces is employed (Figure 7) (7).
- Stress-induced dislocation-like processes within the hydrates result in flow (or long-term) creep strains ε^f. The state of respective microstructural changes is described by the viscous flow γ.
- Stress-induced microdiffusion of water in the capillary pores between the hydrates result in viscous (or short-term) creep strains ε^v.

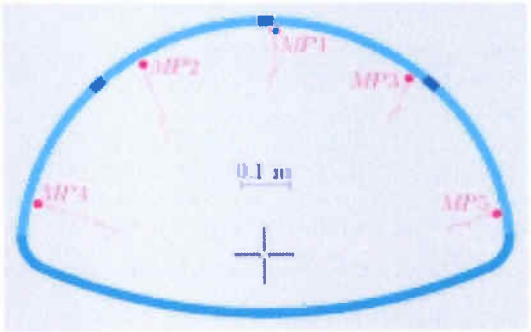

Fig. 6 Displacements measured in the Semmering pilot tunnel at station 4.274: displacement history of the five measurement points for the first 35 days after excavation (circles indicate the location of the measurement points 12 hours, 36 hours, 7 days, and 9 days after excavation).

Bild 6 *Gemessene Verschiebungen beim Semmering-Pilotstollen (km 4.274): Lage der Mepunkte whrend der ersten 35 Tage nach dem Ausbruch (Kreise bezeichnen die Lage der Mepunkte nach 12 Stunden, 36 Stunden, 7 Tagen und 9 Tagen nach dem Ausbruch).*

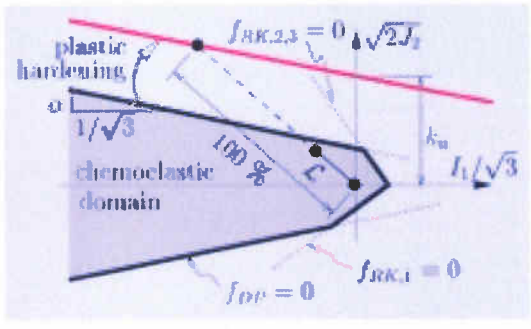

Fig. 7 Multisurface plasticity model consisting of Drucker-Prager loading surface and three Rankine loading surfaces (7).

Bild 7 *Vielflchenplastizittsmodell bestehend aus einer Drucker-Prager- und drei Rankine-Versagensflchen (7).*

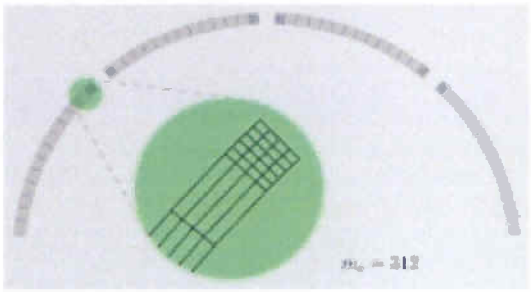

Fig. 8 Semmering pilot tunnel: FE mesh (m_e: number of finite elements).

Bild 8 *Semmering-Pilotstollen: FE-Netz (m_e: Anzahl der finiten Elemente).*

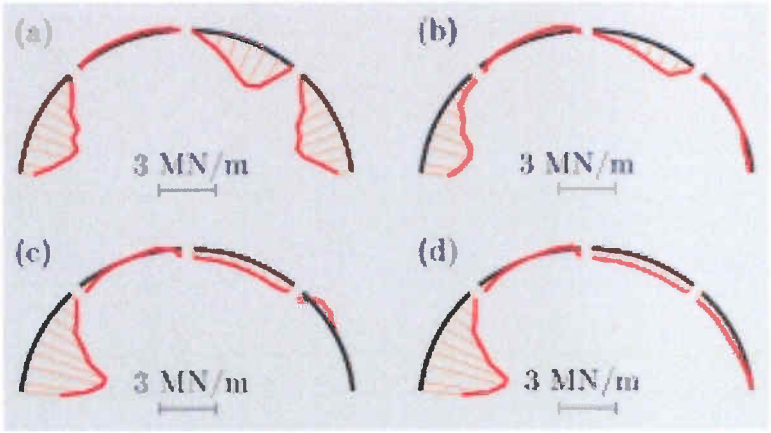

Fig. 9 Semmering pilot tunnel: distribution of the axial forces in the circumferential direction for (a) t = 12 hours, (b) t = 36 hours, (c) t = 7 days, and (d) t = 9 days.

Bild 9 *Semmering-Pilotstollen: Verteilung der Normalkrfte in Umfangsrichtung nach (a) t = 12 Stunden, (b) t = 36 Stunden, (c) t = 7 Tagen, and (d) t = 9 Tagen.*

Representative results of finite element analyses

The finite element discretization employed in the chemomechanical analysis is shown in Figure 8. It consists of 312 bilinear finite elements. Smaller elements were used in the vicinity of the shotcrete-LSC interfaces. In these areas, a significant shear transfer from the rock to the shotcrete lining is expected.

The following interpretation of results is supported by three figures:

- Figure 9 shows the spatial distribution of the circumferential axial forces (MN/m) for selected time instants. These force are computed from the circumferential stresses σ_φ as

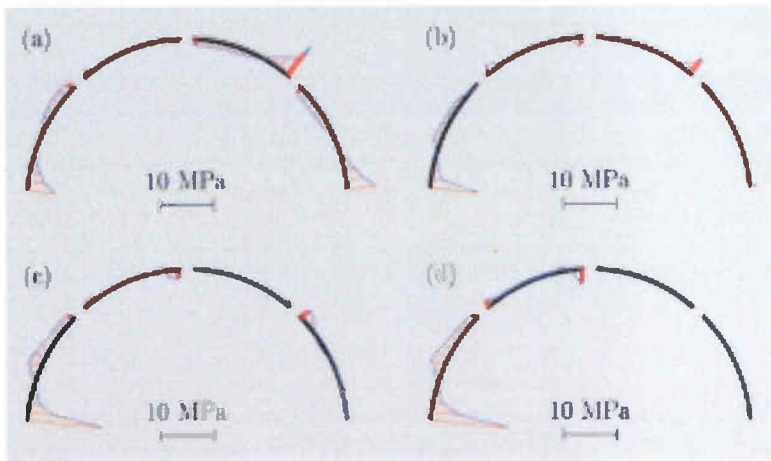

Fig. 10 Semmering pilot tunnel: distribution of the shear stresses at the shotcrete-rock interface for (a) t = 12 hours, (b) t = 36 hours, (c) t = 7 days, and (d) t = 9 days.

Bild 10 *Semmering-Pilotstollen: Verteilung der Schubspannungen an der Grenzfläche zwischen Spritzbeton und Fels nach (a) t = 12 Stunden, (b) t = 36 Stunden, (c) t = 7 Tagen, and (d) t = 9 Tagen.*

$$n_\varphi = \int_h \sigma_\varphi dr \quad \text{.....[1]}$$

with h as the thickness of the tunnel lining.

- Figure 10 shows the shear stresses $\sigma_{r\varphi}$ at the shotcrete-rock interface. They are determined from the reaction forces at the nodes of the exterior surface of the tunnel lining.
- Finally, Figure 11 shows the spatial distribution of an estimate of the safety of the structure ("degree of utilization", "level of loading"), based on failure of concrete in the uni- or biaxial compressive domain, described by means of the Drucker-Prager surface (see Figure 7) namely

$$\bar{L}(\varphi, t) = \frac{1}{h}\int_h L(r, \varphi, t)dr \quad \text{.....[2]}$$

$$L = \frac{\alpha I_1 + |s|}{k_u} \quad \text{.....[3]}$$

with

I_1 the first invariant of the stress tensor,

$|s| = \sqrt{s_{ij}s_{ij}}$ the norm of the stress deviator,

α, k_u material parameters for the Drucker-Prager yield surface (see Figure 7).

In order to assess the states of stress in the tunnel lining, it is instructive to consider the displacements given at the measurement points (see Figure 6). MP2 and MP4 exhibit larger radial displacements than all other MPs. Moreover, a circumferential shift of MP2 towards MP4 is observed. Therefore, large forces n_φ prevail in the left lower tunnel segment for all time instants considered in Figure 9. These axial forces are induced by large shear stresses at the shotcrete-rock-interface (see Figure 10). It is assumed, that these shear stresses are mainly transferred by the anchor bolts forming a relatively dense pattern (see Figure 1a). The unsymmetrical deformation of the tunnel is most likely caused by the rock mass structure, respectively the schistosity. This results in computed tensile forces over the major part of the upper left segment. The respective values of numerically obtained quantities are bounded because of the employed Rankine failure criterion.

The right upper segment shows compressive forces n_φ, induced by the shear stresses at the interface. However, except from relatively early stages (t = 12 h), they do not reach the magnitude of the forces in the left lower segment: Since the inward movement of the rock is less pronounced here than in the left lower part of the tunnel cross section, short-term creep of shotcrete leads to a relaxation of the forces n_φ.

The right lower segment shows relatively low loads except at a very early stage.

In the course of the loading history of the measurement cross section at km 4.274, significant in-plane bending moments

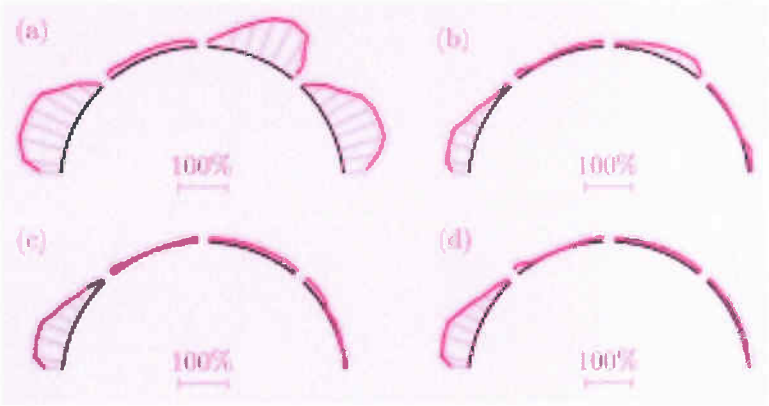

Fig. 11 Semmering pilot tunnel: distribution of the level of loading for (a) t = 12 hours, (b) t = 36 hours, (c) t = 7 days, and (d) t = 9 days.

Bild 11 *Semmering-Pilotstollen: Verteilung des Auslastungsgrads nach (a) t = 12 Stunden, (b) t = 36 Stunden, (c) t = 7 Tagen und (d) t = 9 Tagen.*

$$m_\varphi = \int_h \sigma_\varphi (r - r_0) dr \quad \text{.....[4]}$$

are occurring, with r_0 indicating the middle lining surface. This follows from $6\, m_\varphi/(n_\varphi\, h) > 1$, i.e. the resulting axial force n_φ may be outside the kernel of the cross section. This is illustrated in Figure 12, referring to the time instant of 12 h after lining installation.

The negative bending moments at the lower edges of the left lower segment and of both right segments reflect the (local) introduction of compressive forces from the rock-shotcrete interface into the tunnel lining (see Figure 12c). All positive moments are stemming from curvatures induced by the deformation of the rock. Interestingly, the sign of these moments is opposite to the ones reported in earlier work on the same tunnel support system (13). There, each segment was regarded as a beam on two supports. In view of the present results, this seems to be an incorrect assumption. The eccentricity m_φ/n_φ reflects both the introduction of forces from the rock-shotcrete interface into the tunnel lining and bending loading induced by the deformation of the rock. Also, in contrast to the statements reported in (13), the eccentricity may either increase or decrease with increasing distance from a longitudinal gap (see Figure 12b).

As for the LSCs, they enlarge the circumferential forces in the gaps from zero (corresponding to a situation characterized by longitudinal gaps without LCSs) to a value smaller than the compressive strength of shotcrete. However, in the case studied in this work this value is by far smaller than the maximum circumferential axial force prevailing in some of the shotcrete segments. The latter presumably are induced mainly by the anchor bolts. It appears that the LSCs in the case studied did not contribute very much to the stress of the lining. Their influence seems to be rather local, i.e., in the vicinity of the longitudinal gaps. Higher capacity LSCs could have been installed without problem, which would presumably have increased the support resistance.

Remarkably, the degree of utilization $\bar{L}$ locally reaches values up to 1 (see Figure 11). For the lining being a sealing device rather than a load-driven structure, this situation does not cause failure, although it is not desirable in view of the safety of the crew. In order to avoid $\bar{L} = 1$, more than three longitudinal gaps are probably needed.

Conclusions

The numerical analysis of the Semmering pilot tunnel has shown that in this particular case the LSCs most probably have been underdesigned and thus have only a local influence on the axial forces in the circumferential direction of the tunnel lining. The loading of the lining seems to be mainly controlled by the rock bolts at the shotcrete-rock interface enabling the transfer of shear stresses from rock to shotcrete. This stress transfer results in both tensile and compressive loading of the lining. Stronger LSCs in combination with more gaps would reduce the shear loading of the rock bolts due to reduced relative displacement between rock mass and lining. This would have the positive effect, that the risk of failure of the bolt head, which is often observed in tunnels in squeezing rock, would be reduced as well.

The numerical results have confirmed that in this special case the rock bolt reinforced rock mass stabilizes without a greater contribution of the lining. In this case, the lining served as a sealing device of the rock rather than as a means of support. This also implies that, most likely, the deformations have not been much influenced by the lining.

On the basis of the obtained numerical results the main conclusion is as follows: The longitudinal gaps in the tunnel lining are essential to prevent the destruction of the lining under the observed deformation. The LSCs provide an additional transfer of axial forces across the longitudinal gaps resulting in an improved utilization of the shotcrete lining. Increasing the influence of the LSCs on the global load-carrying behaviour of the support system under the investigated conditions would require

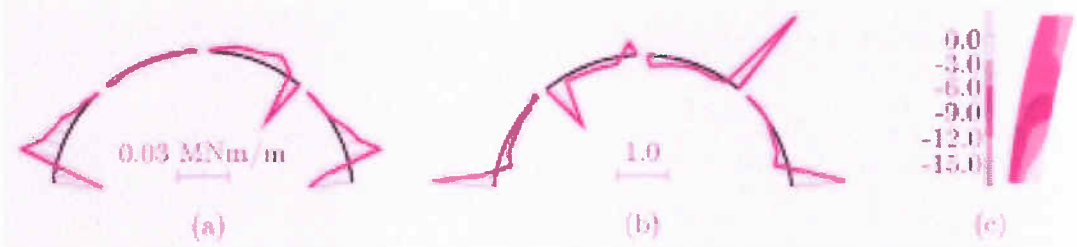

Fig. 12 Semmering pilot tunnel: distribution of (a) the in-plane bending moments m_φ and (b) the normalized eccentricity $6\, m_\varphi/(h\, n_\varphi)$ at t = 12 h; (c) introduction of forces at lower edge of left lower segment illustrated by the distribution of the circumferential stresses σ_φ (in MPa).

Bild 12 *Semmering-Pilotstollen: Verteilung (a) der Biegemomente m_φ in der Tunnelquerschnittsebene und (b) der normierten Exzentrizitt $6\, m_\varphi/(h\, n_\varphi)$ nach t = 12 Stunden; (c) Krafteinleitung am unteren Ende des linken unteren Segments, dargestellt anhand der Verteilung der Umfangsspannungen σ_φ (in MPa).*